Facile synthesis of chitosan nanoparticle-modified MnO_2 nanoflakes for ultrafast adsorption of Pb(II) from aqueous solution

Tianli Han, Xiaoman Zhang, Xiangqian Fu and Jinyun Liu

ABSTRACT

Chitosan nanoparticle (CS NP)-modified MnO_2 nanoflakes were presented as a novel adsorbent for fast adsorption of Pb(II) from aqueous solution. Loading dense CS NPs onto mono-dispersive flower-like MnO_2 nanostructures reduces the overlap of CS during adsorption, and thus improves the contact of functional adsorption sites on the surface of MnO_2 nanoflakes with heavy metal ions. The results show that the removal efficiency of the nanoadsorbents reaches up to 93% in 3 min for Pb(II). In addition, the maximum adsorption capacity, effects of adsorbent dosage and pH value, and the reusability were investigated. The kinetic process and adsorption isotherm fit well with the pseudo-second-order model and Langmuir model, respectively. These findings provide a potential strategy to address the overlap issue of some common nanoadsorbents.

Key words | adsorption, heavy metal ions, nanoparticles, removal, surface modification

Tianli Han†
College of Chemistry and Material Engineering,
Chaohu University,
Chaohu, Anhui 238000,
China

Xiaoman Zhang†
Xiangqian Fu
Jinyun Liu (corresponding author)
Nanomaterials and Environment Detection Laboratory,
Institute of Intelligent Machines, Chinese Academy of Sciences,
Hefei, Anhui 230031,
China
E-mail: *jyliu@iim.ac.cn*

Xiaoman Zhang
Xiangqian Fu
Department of Chemistry,
University of Science and Technology of China,
Hefei, Anhui 230026,
China

Jinyun Liu
Beckman Institute for Advanced Science and Technology,
University of Illinois at Urbana-Champaign,
Urbana, IL 61801,
USA

†These authors contribute equally to this work.

INTRODUCTION

Heavy metal ions in water are severely harmful to human health (Repo *et al.* 2013; Carpenter *et al.* 2015; Chiavola *et al.* 2015; Gupta *et al.* 2016). For example, it has been confirmed that Pb(II) increases the risk of cancer and intelligence defects (Clausen *et al.* 2011; Bhatluri *et al.* 2015; Du *et al.* 2016; Jiang *et al.* 2016). The efficient removal of heavy metal ions from aqueous solution is significant. In recent years, among many other approaches (such as membrane filtration and ion exchange), adsorption of pollutants from water by utilizing adsorbents has attracted broad attention because of its low cost and easy operation, etc. (Chen *et al.* 2013; Yin *et al.* 2013; Raychoudhury *et al.* 2015; Rodriguez-Flores *et al.* 2015). However, the adsorption rate and capacity of many adsorbents are as yet non-ideal, which limits the applications of adsorbents, especially for the purification of drinking water. Recently, nanomaterials with large surface area and functional groups which can capture pollutants specifically have been considered promising adsorbents (Liu *et al.* 2015; Sharma *et al.* 2015; Adeleye *et al.* 2016).

Chitosan (CS), which is derived from the deacetylation of chitin, possesses many fascinating features including abundance, multifunctionality, and non-toxicity (Sowasod *et al.* 2013; An *et al.* 2015; Sun *et al.* 2016). CS is considered to be a promising material for adsorption of heavy metal ions from water due to its special molecular structure, which contains a lot of amino and hydroxyl groups. However, CS aggregates in solution easily, which limits its potential applications. Despite many significant efforts focused on the cross-linking and modification of CS,

doi: 10.2166/ws.2016.109

reducing aggregation and improving the effective surface area exposed to pollutants remain a great challenge.

In a solution environment without sufficient stirring, CS nanoparticles (NPs) would aggregate and overlap due to the requirement of automatically reducing surface energy (Anson *et al.* 2004; Michiardi *et al.* 2007), resulting in the adsorption sites located in deep positions being covered by the top layer. In this condition, many adsorption sites can hardly be effective at contacting and adsorbing surrounding heavy metal ions. Here, we present a promising strategy to address the overlap issue of CS during adsorption. In our investigation, CS NPs are loaded onto a flower-like MnO_2 nanostructure which is chemically stable and monodispersive. The flower-like MnO_2 with its branched morphology keeps sufficient spaces between adjacent MnO_2 materials, providing good conditions to ensure CS NPs located on each petal are well exposed to the surroundings. This adsorbent possesses the following features: (1) the aggregation of CS is effectively reduced due to the support of the three-dimensional (3D) flower-like MnO_2, enabling the functional groups of CS to be exposed to heavy metal ions (Pb(II) was employed here); (2) the size of CS NPs is small, which means the CS possesses high surface area and high reactivity for chemically binding with Pb(II); (3) the structure of the adsorbents is stable because of the chemical stability of MnO_2, and thus the adsorbents can remove heavy metal ions in neutral drinking water.

METHODS

The preparation procedure for MnO_2 nanoflakes is similar to that described in a previous report (Zhang *et al.* 2013) with some modifications. Typically, 2 mmol of $MnSO_4{\cdot}H_2O$ and 2 mmol $K_2S_2O_8$ were dissolved into 35 mL of de-ionized water under stirring for 30 min. The obtained solution was transferred to a Teflon-lined stainless steel autoclave, which was subsequently sealed and heated in an oven at 150 °C for 30 min. After naturally cooling down, the black precipitates were collected and washed alternately with water and ethanol. At last, the as-prepared samples were dried in a vacuum oven at 60 °C for 5 h.

In order to modify the MnO_2 nanoflakes with CS NPs, the following steps were conducted. First, 0.1 mL of CH_3COOH was added into 40 mL of de-ionized water to form a homogeneous solution. Then, 0.04 g of CS was added into the solution under stirring until clarification. After that, 0.05 g of MnO_2 nanoflakes was put into the solution under stirring for 30 min. Na_2CO_3 was used for adjusting the pH value to 8 to nucleate the CS particles. Finally, after stirring for an additional 30 min, the samples were collected and washed with water, and dried in a vacuum oven at 60 °C for 3 h.

The samples were characterized by using a Philips X'Pert Pro X-ray diffractometer (XRD), an FEI Sirion 200 field emission scanning electronic microscope (FESEM), and a JEOL JEM-2010 transmission electron microscope (TEM). Fourier transform infrared (FTIR) spectra were recorded on a Shimadzu IR-440 spectrometer. Surface area was measured on a Coulter Omnisorp 100CX Brunauer–Emmett–Teller (BET).

Pb(II) was used as the target heavy metal ion for adsorption. In a typical procedure, 20 mL Pb(II) aqueous solutions, prepared by dissolving $Pb(NO_3)_2$ (Sigma-Aldrich Corp. without further purification) into de-ionized water at different concentrations ranging from ~10 to 400 mg L^{-1}, were dispersed with 20 mg of the as-obtained adsorbents. All adsorption was conducted in a vibration water bath at 25 °C. After a certain period of adsorption time, the solutions were separated and collected by centrifuge. The remaining concentrations of Pb(II) were measured by a Jarrell-Ash ICAP-9000 inductively coupled plasma. For the investigation of the adsorption effect of adsorbent dosage, series amounts of adsorbent ranging from 0.1 to 2 g L^{-1} were used, while the initial concentration of Pb(II) and adsorption time were 20 mg L^{-1} and 2 h for each adsorption, respectively. In pH-dependent adsorptions (initial concentration of Pb(II): 10 mg L^{-1}; adsorption time: 3 h), pH values ranged from 2 to 6, and were adjusted by 0.5 M HCl or NaOH solutions.

RESULTS AND DISCUSSION

In FESEM images (Figure 1(a) and 1(b)), the MnO_2 nanoflakes exhibit a spherical flower-like morphology. Several nanoflakes assemble around a core, exhibiting a whole architecture in a diameter of ~2 μm. The thickness of each

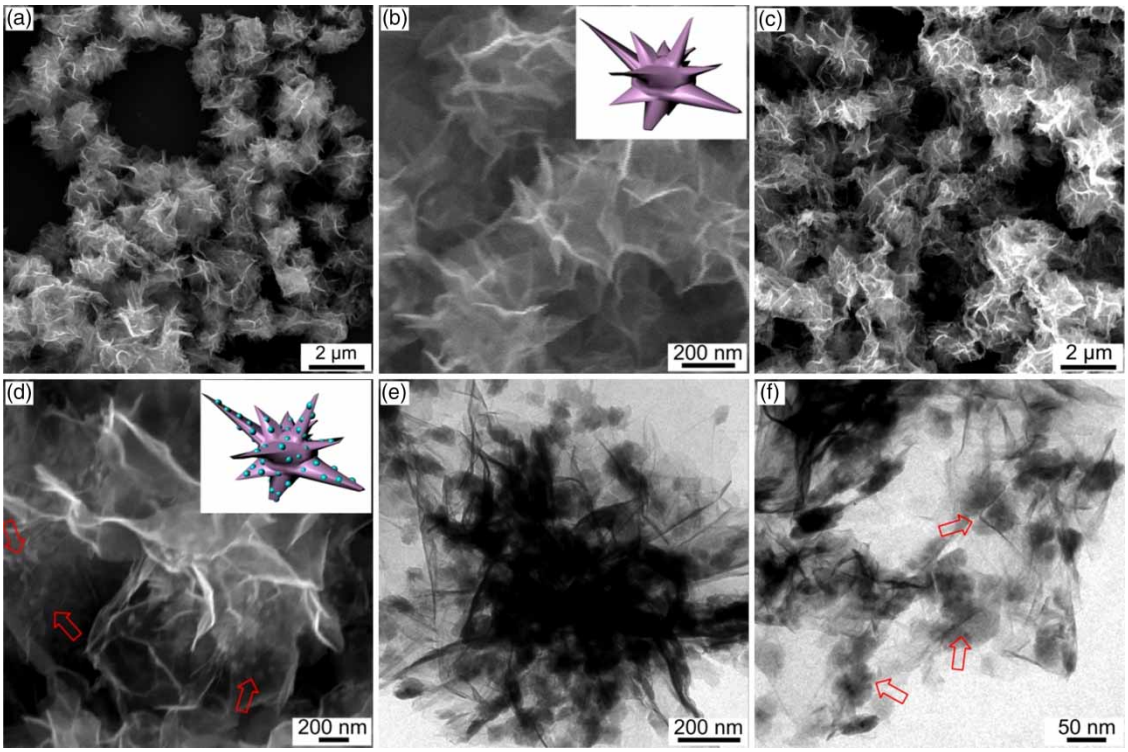

Figure 1 | (a) Low- and (b) high-magnification FESEM images of the MnO_2 nanoflakes; (c), (d) FESEM images and (e), (f) TEM images of the MnO_2 nanoflakes modified with CS NPs. Insets in (b) and (d) are corresponding schematic illustrations of nanoflakes without and with NP modifications, respectively.

nanoflake is around 5 to 8 nm. After modifying with CS, the flower-like morphology kept stable, as shown in Figure 1(c). However, as shown in the high-magnification FESEM image (Figure 1(d)), many NPs were loaded on the surface of each nanoflake. It is indicated that some CS NPs were deposited onto the surface of MnO_2, which is further supported by the TEM observations (Figure 1(e) and 1(f)). The size of CS NPs ranges from 45 to 65 nm. The composition of the samples is confirmed by the XRD patterns, as shown in Figure 2. All peaks are well indexed to the MnO_2 phase (JCPDS card No. 80–1098) without any impurities. The diffraction peaks (2θ) at about 12.6 °, 25.3 °, 37.3 °, 42.6 °, 55.8 °, and 67.1 ° can be assigned to the (001), (002), (111), (112), (113), and (020) crystal planes of birnessite-type MnO_2, respectively. However, it should be noted that there is no obvious XRD signal from CS NPs, which can be ascribed to the small amount of CS within the MnO_2/CS composites. Because of that, further investigation about the composition was conducted through FTIR characterization (Figure 3).

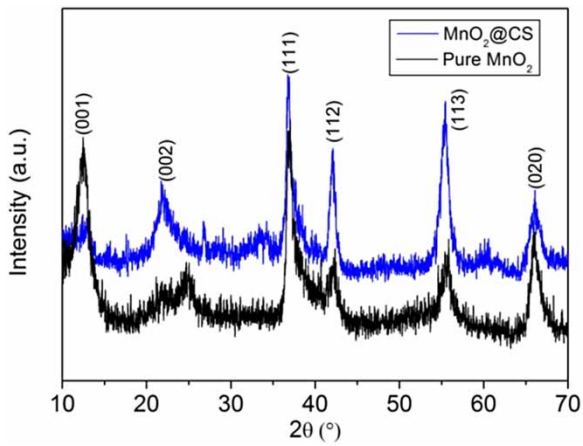

Figure 2 | XRD patterns of the MnO_2 nanoflakes before and after modification with CS NPs.

In Figure 3, the peaks at about 2,870 and 1,410 cm^{-1} can be indexed to the stretching and bending vibrations of C – H, respectively, which rarely appear in pure MnO_2 crystals reported previously (Nand *et al.* 2016; Ramesh *et al.* 2016), indicating the existence of organic components in

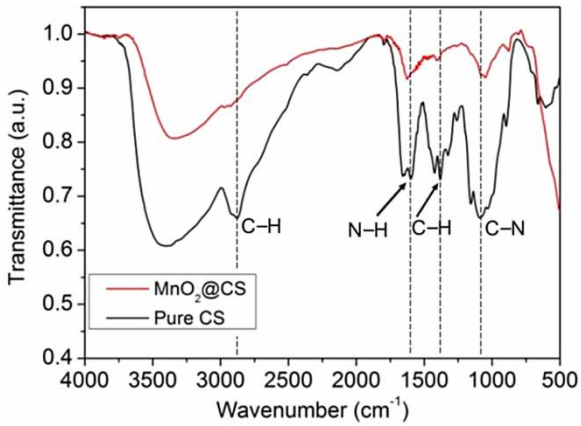

Figure 3 | FTIR spectra of the CS NP-modified MnO_2 nanoflakes and the pure CS.

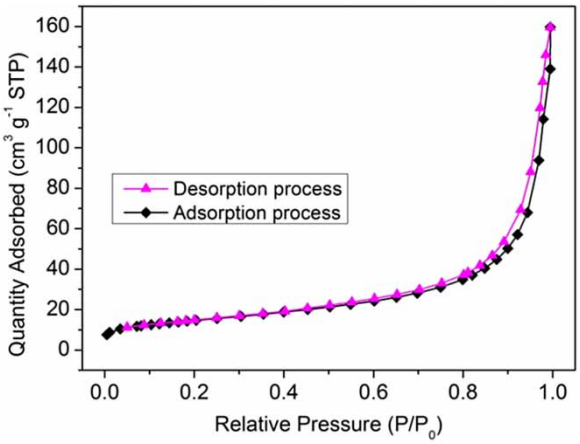

Figure 4 | Typical N_2 adsorption–desorption isotherm of the CS NPs-modified MnO_2 nanoflakes.

the prepared adsorbents. The peak at ~1,150 cm^{-1} is assigned to the characteristic band of C – N stretching vibration, which also supports the modification of MnO_2 nanoflakes with CS. The peak located at about 1,600 cm^{-1} is assigned to the N – H scissor (Colilla *et al.* 2006), which can be attributed to the functional group of CS molecules, since pure MnO_2 lacks this group (Aghazadeh *et al.* 2016). Impressively, this amine group should be able to play a significant role in the adsorption of positive Pb(II). In additional, as shown in Figure 4, the BET surface area is about 73.5 m^2 g^{-1}.

Figure 5 shows the adsorption performance of the CS NP-modified MnO_2 nanoflakes for Pb(II). During the kinetic adsorption process, the initial concentration of Pb(II) is ~10 mg L^{-1}. In Figure 5(a), we can see that the removal efficiency rapidly reaches ~93% in 3 min. It goes up to 98% after 10 min, exhibiting a high adsorption rate. The kinetic process is well fitted with a pseudo-second-order model, as shown in Figure 5(b). The pseudo-second-order model is shown in Equation (1) (Vinod & Anirudhan 2003):

$$\frac{dq_t}{dt} = k_2(q_e - q_t)^2 \quad (1)$$

where k_2 is a pseudo-second-order rate constant. In this model, it is assumed that the difference between the concentration at time t and the saturated adsorption amount (q_e) is the driving force of adsorption.

Figure 6(a) and 6(b) show the saturated adsorption isotherm and the Langmuir model-fitted results, respectively.

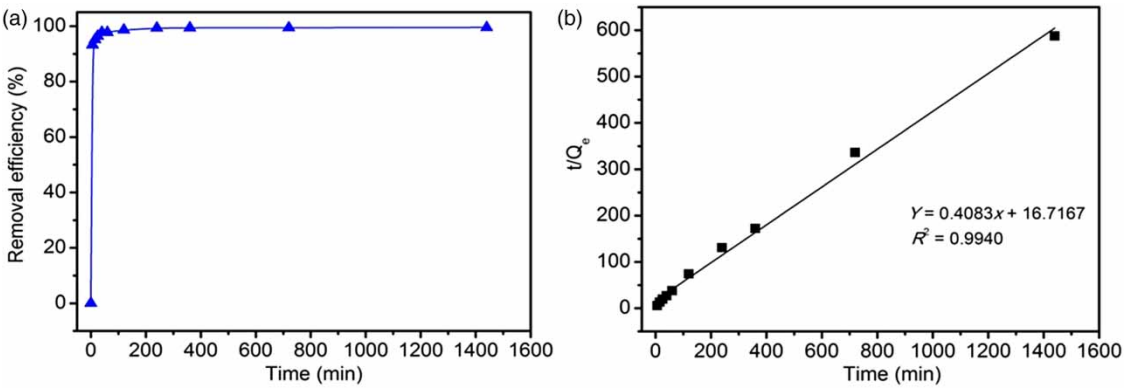

Figure 5 | (a) Relationship between the removal efficiency and adsorption time; (b) the kinetic process fitted with a pseudo-second-order model.

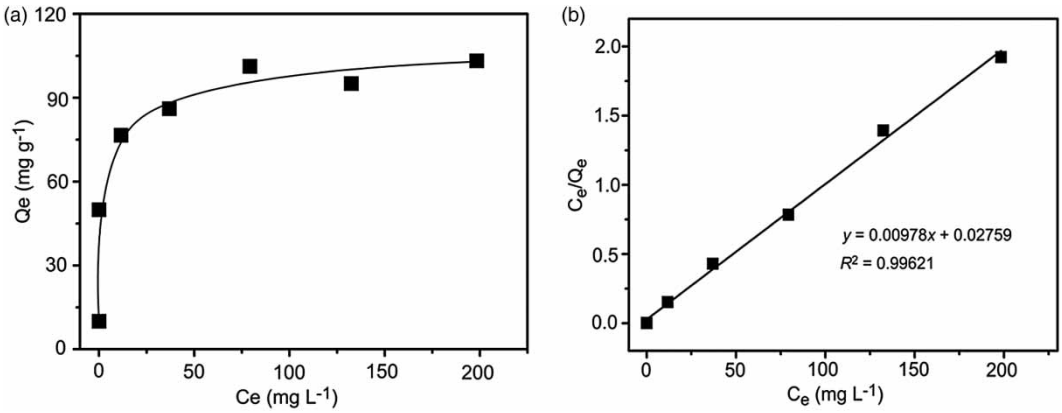

Figure 6 | (a) The saturated adsorption isotherm of the CS NP-modified MnO_2 nanoflakes; (b) the fitting result by a Langmuir isotherm model.

The maximum adsorption capability of the CS NP-modified MnO_2 nanoflakes is ~102.5 mg g^{-1}, far exceeding the MnO_2 nanoflakes without CS NP modification (40.8 mg g^{-1}) and CS bulk (36.6 mg g^{-1}). In addition, both the high adsorption rate and capacity are competitive with some other reports about CS adsorbents (Zhu *et al.* 2012). The good performance can be ascribed to the special CS NP-modified nanostructure which provides a large surface area and numerous well-exposed functional groups to efficiently adsorb Pb(II). Under the support of the 3D flower-like structure, the adsorption sites of CS can expose and capture target ions in solution. About an adsorption mechanism, it would be a complicated interaction including electrostatic attraction and chemical bonding (complexation and

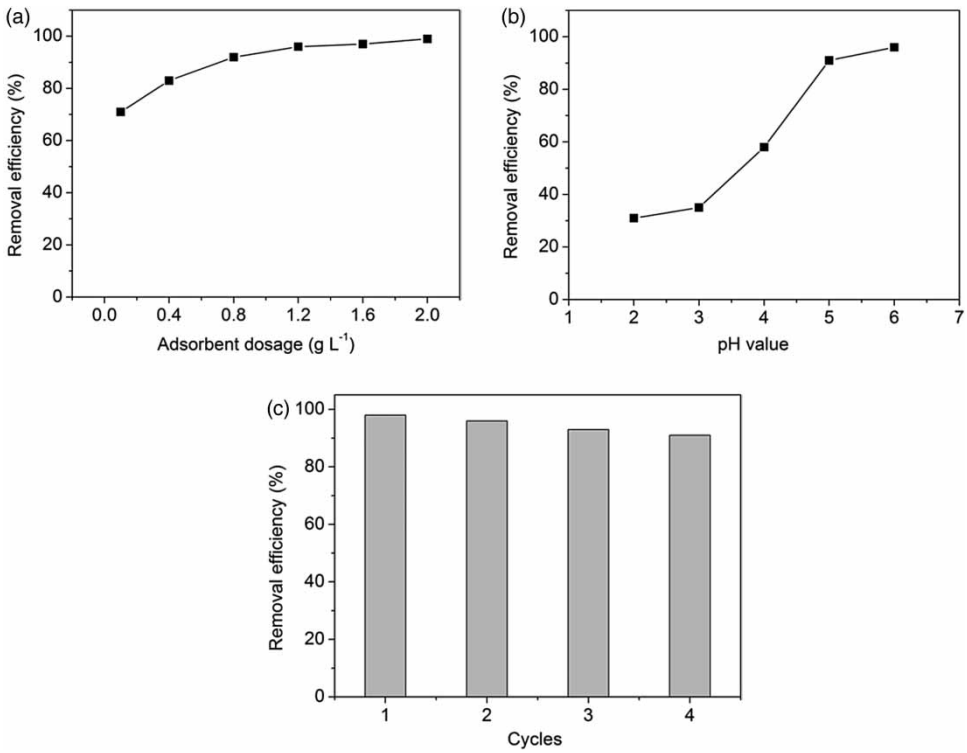

Figure 7 | The effects of (a) adsorbent dosage and (b) pH value on Pb(II) adsorption onto the CS NP-modified MnO_2 nanoflakes. (c) Adsorbent regeneration cycles (conditions: initial concentration of Pb(II): 20 mg L^{-1}; adsorbent dosage: 1 g L^{-1}; adsorption time: 3 h; desorption time: 3 h; 0.05 mol L^{-1} EDTA as regeneration agent).

chelation). Within the CS molecules, there are two chemically active sites (amine and hydroxyl groups) that would participate in the reactions with Pb(II). For example, it was demonstrated that the lone pair of electrons present in the nitrogen of the amine group can be supplied to the empty atomic orbital of metal ions, forming a CS–metal complex (Zhang *et al.* 2016).

In addition, the effects of adsorbent dosage and pH value were investigated. In Figure 7(a), the adsorption efficiency increases depending on the increase of dosage from 0.1 to 1.2 g L^{-1}. It can be ascribed to the increase of adsorption sites and surface area. When the amount of adsorbents becomes excessive, the increase of removal efficiency becomes slow. This is perhaps due to the concentration gradient between solute concentration in solution and the one on the surface of the adsorbents (Vadivelan & Kumar 2005). Figure 7(b) shows the pH-dependent adsorption behavior. While increasing pH to 7.0 results in the precipitation of lead hydroxide (Naiya *et al.* 2008), in our investigations the pH values were lower than 6. In Figure 7(b), low pH value is not favorable for high efficiency. A high pH value increases the deprotonation of the adsorbent surface, forming negatively charged sites, which enhances the attraction between adsorbents and Pb(II) (Nassar 2010). It is indicated the presented adsorbents are more efficient for weak acidic and neutral water purification. Figure 7(c) shows the reusability of the adsorbents. In order to regenerate the CS-modified adsorbents, ethylenediaminetetraacetic acid (EDTA) solution was employed as a strong chelating agent (Yan *et al.* 2012). The removal efficiency slowly decreases with the increase of cycle number; however, the removal percentage still remains above 91% after four cycles, indicating good stability and reusability for Pb(II) adsorption.

CONCLUSIONS

In summary, we present an effective strategy to utilize CS NPs for fast adsorption of Pb(II) from aqueous solution. Dense CS NPs are modified on monodispersive flower-like MnO_2 nanoflakes. The overlap of CS NPs can be significantly reduced, thereby improving the exposure of adsorption sites to heavy metal ions in solution. The adsorbents exhibit a high removal efficiency of about 93% in 3 min for Pb(II), and a maximum adsorption capability around 102.5 mg g^{-1}. The results show that the adsorption efficiency increases depending on the increase of adsorbent dosage; in the range from 2 to 6, a high pH value is favorable for high adsorption efficiency; and the removal percentage remains above 91% after four regeneration cycles. It is expected that the presented nanoadsorbents could be a promising candidate for water purification; and the strategy of loading NP onto flower-like architectures would also stimulate some new studies about high-performance nanoadsorbents.

ACKNOWLEDGEMENTS

This work was financially supported by the State Key Project of Fundamental Research for Nanoscience and Nanotechnology (2011CB933700), and the National Natural Science Foundation of China (51002157, 21277146, 61071054, and 21177131).

REFERENCES

Adeleye, A. S., Conway, J. R., Garner, K., Huang, Y. X., Su, Y. M. & Keller, A. A. 2016 Engineered nanomaterials for water treatment and remediation: costs, benefits, and applicability. *Chemical Engineering Journal* **286**, 640–662.

Aghazadeh, M., Asadi, M., Maragheh, M. G., Ganjali, M. R., Norouzi, P. & Faridbod, F. 2016 Facile preparation of MnO_2 nanorods and evaluation of their supercapacitive characteristics. *Applied Surface Science* **364**, 726–731.

An, B., Lee, H., Lee, S., Lee, S. H. & Choi, J. W. 2015 Determining the selectivity of divalent metal cations for the carboxyl group of alginate hydrogel beads during competitive sorption. *Journal of Hazardous Materials* **298**, 11–18.

Anson, A., Jagiello, J., Parra, J. B., Sanjuan, M. L., Benito, A. M., Maser, W. K. & Martinez, M. T. 2004 Porosity, surface area, surface energy, and hydrogen adsorption in nanostructured carbons. *Journal of Physical Chemistry B* **108**, 15820–15826.

Bhatluri, K. K., Manna, M. S., Ghoshal, A. K. & Saha, P. 2015 Supported liquid membrane based removal of lead(II) and cadmium(II) from mixed feed: conversion to solid waste by precipitation. *Journal of Hazardous Materials* **299**, 504–512.

Carpenter, A. W., Lannoy, C. F. & Wiesner, M. R. 2015 Cellulose nanomaterials in water treatment technologies. *Environmental Science & Technology* **49**, 5277–5287.

Chen, F. X., Xie, S. L., Zhang, J. H. & Liu, R. 2013 Synthesis of spherical Fe_3O_4 magnetic nanoparticles by co-precipitation in choline chloride/urea deep eutectic solvent. *Materials Letters* **112**, 177–179.

Chiavola, A., D'Amato, E., Gavasci, R. & Sirini, P. 2015 Arsenic removal from groundwater by ion exchange and adsorption processes: comparison of two different materials. *Water Science and Technology: Water Supply* **15** (5), 981–989.

Clausen, J. L., Bostick, B. & Korte, N. 2011 Migration of lead in surface water, pore water, and groundwater with a focus on firing ranges. *Critical Reviews in Environmental Science and Technology* **41**, 1397–1448.

Colilla, M., Salinas, A. J. & Vallet, M. 2006 Amino-polysiloxane hybrid materials for bone reconstruction. *Chemistry of Materials* **18**, 5676–5683.

Du, Z. L., Zheng, T., Wang, P., Hao, L. L. & Wang, Y. X. 2016 Fast microwave-assisted preparation of a low-cost and recyclable carboxyl modified lignocellulose-biomass jute fiber for enhanced heavy metal removal from water. *Bioresource Technology* **201**, 41–49.

Gupta, V. K., Moradi, O., Tyagi, I., Agarwal, S., Sadegh, H., Shahryari-Ghoshekandi, R., Makhlouf, A. S. H., Goodarzi, M. & Garshasbi, A. 2016 Study on the removal of heavy metal ions from industry waste by carbon nanotubes: effect of the surface modification: a review. *Critical Reviews in Environmental Science and Technology* **46**, 93–118.

Jiang, H. Y., Zhao, Q. X. & Zeng, Y. 2016 Removal of Cd(II) and Pb(II) from aqueous solutions by modified polyvinyl alcohol. *Desalination and Water Treatment* **57**, 6452–6462.

Liu, P., Borrell, P. F., Bozic, M., Kokol, V., Oksman, K. & Mathew, A. P. 2015 Nanocelluloses and their phosphorylated derivatives for selective adsorption of Ag^{+}, Cu^{2+} and Fe^{3+} from industrial effluents. *Journal of Hazardous Materials* **294**, 177–185.

Michiardi, A., Aparicio, C., Ratner, B. D., Planell, J. A. & Gil, J. 2007 The influence of surface energy on competitive protein adsorption on oxidized NiTi surfaces. *Biomaterials* **28**, 586–594.

Naiya, T. K., Bhattacharya, A. K. & Das, S. K. 2008 Adsorption of Pb(II) by sawdust and neem bark from aqueous solutions. *Environmental Progress* **27**, 313–328.

Nand, B., Pradhan, A. C. & Parid, K. M. 2016 A comparative study on adsorption and photocatalytic dye degradation under visible light irradiation by mesoporous MnO_2 modified MCM-41 nanocomposite. *Microporous and Mesoporous Materials* **226**, 229–242.

Nassar, N. N. 2010 Rapid removal and recovery of Pb(II) from wastewater by magnetic nanoadsorbents. *Journal of Hazardous Materials* **184**, 538–546.

Ramesh, M., Nagaraj, H. S., Rao, M. P., Anandan, S. & Huang, N. M. 2016 Fabrication, characterization and catalytic activity of α-MnO_2 nanowires for dye degradation of reactive black 5. *Materials Letters* **172**, 85–89.

Raychoudhury, T., Schiperski, F. & Scheytt, T. 2015 Distribution of iron in activated carbon composites: assessment of arsenic removal behavior. *Water Science and Technology: Water Supply* **15** (5), 990–998.

Repo, E., Warchol, J. K., Bhatnagar, A., Mudhoo, A. & Sillanpa, M. 2013 Aminopolycarboxylic acid functionalized adsorbents for heavy metals removal from water. *Water Research* **47**, 4812–4832.

Rodriguez-Flores, L., Marmolejo-Santillan, Y., Perez-Moreno, F., Castaneda-Ovando, A., Sierra-Zenteno, A., Flores-Castro, K. & Cadena-Zamudio, J. L. 2015 Adsorption of arsenic in dacitic tuff pretreated with magnesium oxide. *Water Science and Technology: Water Supply* **15** (1), 181–187

Sharma, V. K., Zboril, R. & Varma, R. S. 2015 Ferrates: greener oxidants with multimodal action in water treatment technologies. *Accounts of Chemical Research* **48**, 182–191.

Sowasod, N., Nakagawa, K., Charinpanitkul, T. & Tanthapanichakoon, W. 2013 Encapsulation of curcumin loaded oil droplets with chitosan based cryogel: influence of freezing condition on nanocapsule properties. *Food Science and Technology Research* **19**, 633–640.

Sun, X. T., Yang, L. R., Dong, T. T., Liu, Z. N. & Liu, H. Z. 2016 Removal of Cr(VI) from aqueous solution using amino-modified Fe_3O_4-SiO_2-chitosan magnetic microspheres with high acid resistance and adsorption capacity. *Journal of Applied Polymer Science* **133**, 43078.

Vadivelan, V. & Kumar, K. V. 2005 Equilibrium, kinetics, mechanism, and process design for the sorption of methylene blue onto rice husk. *Journal of Colloid and Interface Science* **286**, 90–100.

Vinod, V. P. & Anirudhan, T. S. 2003 Adsorption behaviour of basic dyes on the humic acid immobilized pillared clay. *Water, Air, & Soil Pollution* **150**, 193–217.

Yan, H., Yang, L. Y., Yang, Z., Yang, H., Li, A. M. & Cheng, R. S. 2012 Preparation of chitosan/poly(acrylic acid) magnetic composite microspheres and applications in the removal of copper(II) ions from aqueous solutions. *Journal of Hazardous Materials* **229**, 371–380.

Yin, C. Y., Wei, Y. J., Wang, F. W., Chen, Y. H. & Bao, X. 2013 Magnetic hierarchical porous carbon sphere prepared for removal of organic pollutants in water. *Materials Letters* **104**, 64–67.

Zhang, X., Yu, P., Zhang, H. T., Zhang, D. C., Sun, X. Z. & Ma, Y. W. 2013 Rapid hydrothermal synthesis of hierarchical nanostructures assembled from ultrathin birnessite-type MnO_2 nanosheets for supercapacitor applications. *Electrochimica Acta* **89**, 523–529.

Zhang, L., Zeng, Y. X. & Cheng, Z. J. 2016 Removal of heavy metal ions using chitosan and modified chitosan: a review. *Journal of Molecular Liquids* **214**, 175–191.

Zhu, Y. H., Hu, J. & Wang, J. L. 2012 Competitive adsorption of Pb(II), Cu(II) and Zn(II) onto xanthate-modified magnetic chitosan. *Journal of Hazardous Materials* **221**, 155–161.

First received 16 March 2016; accepted in revised form 10 June 2016. Available online 24 June 2016